Development of an Application to Evaluate the Effect of Headborne Equipment on Warfighter Burden

M. Vignos[1], M. Tumperi[1], M. Yates[1], C. Hanley[1], B. Lindsey[1], N. Thomas[1], G. Holt[1], K. Ott[1], H. Kowpak[1], J. Moramarco[1], A. Gonzalez[1], B. Tate[1], C. Pyles[1], J. Hopping[2], and Q. Luong[1]

[1]The Johns Hopkins University Applied Physics Laboratory, 11100 Johns Hopkins Rd, Laurel, MD, USA, 20723
mike.vignos@jhuapl.edu
[2]Program Executive Office Soldier, 10170 Beach Road, Fort Belvoir, VA, USA, 22060

Abstract. The added mass of personal protective equipment can negatively affect warfighter injury risk and performance. Specifically, the mass properties of headborne equipment (HBE) influence neck mechanics, marksmanship performance, and neck pain and discomfort. This indicates the importance of considering the effect of HBE mass properties on musculoskeletal burden in the design and evaluation of HBE. Thus, the objective of this work was to develop a software application to allow users to evaluate the effect of HBE on musculoskeletal burden, while considering physiological variations across warfighters. This application uses musculoskeletal models to evaluate changes in biomechanical metrics of musculoskeletal burden. The models used in this application were developed from a previously validated whole-body musculoskeletal model. This model was then scaled to the statures, weights, and strengths of a 50th percentile female and male. The ability to vary neck muscle strength from a 5th percentile female to a 95th percentile male was then incorporated using the neck muscle strength of healthy individuals. A model of HBE with the ability to vary mass properties was rigidly attached to the skull. A model of skeletal muscle fatigue was then calibrated using neck muscle fatigue data. This allowed users to model neck muscle fatigue that develops while wearing HBE. Simulations of walking, running, and static prone were implemented using previously collected data. These models and simulations were then packaged into a software application to simulate variations in HBE mass properties, biological sex, activity, strength, and muscle fatigue. This application was then used to investigate the effects of varying HBE mass properties and fatigue. It was found that increasing HBE mass, shifting the centre of mass anterior, and increasing levels of fatigue each led to increased neck joint impulse. This indicates that each of these parameters should be considered in the design and use of HBE.

1. INTRODUCTION

Soldiers wear personal protective equipment (PPE) to protect from blunt, ballistic, and blast events. Of this PPE, helmets serve as a mounting point for performance-enabling equipment, such as heads-up displays, communication devices, night vision devices, and additional armour. However, this headborne equipment (HBE) fundamentally alters the biomechanics of the neck. While HBE is designed to improve performance, HBE may also put warfighters at risk for acute and chronic injury and, potentially, decreased performance, particularly during long-duration operations in which fatigue and discomfort can start to affect warfighters. Specifically, variations in HBE mass properties can negatively impact neck pain and discomfort [1–3], marksmanship performance [3, 4], task concentration and focus [5], and neck muscle fatigue [6]. Much of the prior research has focused on short-duration timescales and, thus, the potentially increasing effects of HBE during long-duration missions are unknown. These risks associated with HBE indicates the need for improved guidance for HBE mass properties.

Recent HBE research has transitioned from a focus on design of flight helmets [7, 8] to the effects of HBE during dismounted operations to inform improved HBE guidance. This research has found that changing HBE mass properties can affect marksmanship performance, neck fatigue, pain/discomfort, user acceptance, and muscle activity [2, 4]. The information from these studies can be used to start to develop guidance for HBE mass properties for dismounted operations [2, 3]. However, experimental limitations make it challenging to use these data alone to develop complete guidance for HBE mass properties. In particular, certain biomechanical and physiological metrics, such as joint reaction forces, are very challenging or impossible to quantify experimentally. This limits our knowledge on the effect of HBE on the musculoskeletal system. Experiments with human participants can also only be used to evaluate the effect of HBE to a limit due to ethical limitations with inducing severe fatigue and high injury risk, which limits the ability to establish a threshold for HBE guidance. Lastly, the time required for experiments poses a challenge for rapid evaluation of new or exploratory HBE.

Computational modelling provides a complementary capability to experiments and overcomes many of the above limitations. In particular, musculoskeletal (MSK) models can be used to evaluate the

https://doi.org/10.52202/081621-0023

effect of external loads on biomechanical response and, thus, provides a method to directly assess the effect of HBE on MSK burden. MSK models have been used to determine that cervical spine motion during target acquisition and head-neck posture may affect neck pain, joint mechanics, and muscle fatigue more than HBE mass properties [9]. This indicates that the scenario is important to consider in HBE mass property guidance for warfighters. However, this prior research focused on a 50th percentile male and simulated relatively simple movements. This limits our understanding of how variations across warfighters during operational movements interact with HBE to affect MSK burden. Additionally, existing MSK models do not incorporate muscle fatigue, which prevents investigations into the effect of mission duration on MSK burden. Further, use of MSK models requires expertise in MSK modelling software and biomechanics. This makes it challenging for operationally-focused individuals to use these tools to evaluate the effect of HBE on MSK burden when assessing equipment trade-offs.

The overall goal of this project was to develop a software application to enable users to evaluate the effect of HBE on warfighter burden while overcoming the limitations of existing MSK models. To achieve this goal, the objectives were to (1) improve existing MSK models to more easily allow for an understanding of the effect of HBE, biological sex, activity, strength, and muscle fatigue on MSK burden, (2) integrate the updated MSK models and analyses into a software application, and (3) use this software application to investigate the effect of HBE mass properties and muscle fatigue on MSK burden.

2. DEVELOPMENT OF THE SOFTWARE APPLICATION

2.1 Development of 50th Percentile Female and Male MSK Models

A previously validated MSK model implemented in OpenSim (Simbios, Stanford, CA) with a detailed representation of the cervical spine was selected as the starting model [10–13]. This model was selected based on its prior validation for analyses used to evaluate MSK burden with MSK models. A rigid model of HBE was then attached to the skull of this model through a fixed joint. The hyoid muscle group was added to the model using previously established muscle definitions to improve the flexion moment-generating capacity of the baseline model [10]. The height and weight of this model was then scaled to 50th percentile male and female models using uniform scaling and preserved mass distribution to align with measurements previously reported for the United States Army [14].

The neck muscle strengths of the 50th percentile models were also scaled to that of an average female and male [15]. This was done by first evaluating the models' maximum isometric strength in flexion and extension about T1-C7 using a modified version of the approach developed by Mortensen et al. [16]. The kinematics of the model were first constrained for all joints except those in the cervical spine. The kinematics of the cervical spine were prescribed to maintain a neutral, upright posture. A 3D linear reserve actuator was applied at the T1-C7 joint to prevent translation of the base of the cervical spine. The strength of the model's neck flexor muscles was measured by applying a 300 N posterior force to the front of the skull and a residual actuator in the opposite direction. The residual force and muscle activations necessary to maintain a neutral cervical spine were then calculated using computed muscle control (CMC) [17]. The difference between the 300 N force and residual actuator force was used to compute the resultant force on the skull. This resultant force vector was then used with a vector from the centre of the T1-C7 joint to the point of force application to compute the models' flexion moment-generating capacity. This process was repeated with a 300 N anterior force and a residual actuator applied to the back of the skull to compute the extension moment-generating capacity of the models. This provided the models' maximum isometric neck flexion and extension strengths, which were then scaled to match the average strength of healthy males and females [18]. This scaling was done by first multiplying the maximum isometric force of the neck muscles by a scale factor computed as the target strength of the model divided by the initial strength. The flexion and extension strengths of the model were then recalculated with the scaled neck muscles. This process was repeated until the model strength was within 0.001% of the target strength. The final 50th percentile male model strength was 52 Nm and 20 Nm in extension and flexion, respectively. The final 50th percentile female model strength was 21 Nm and 15 Nm in extension and flexion, respectively. This provided a female and male model with 50th percentile height, weight, and neck muscle strength.

The ability to model variations in neck muscle strength was then implemented by developing strength-scaling functions to continuously scale the 50th percentile models between 5th and 95th percentile individuals. These functions were developed by first creating normal distributions of the maximum isometric strength for neck flexion and extension of healthy females and males [18]. These distributions were then used to compute target strengths in 5-percentile increments. The maximum isometric force of the neck flexor and extensor muscles of the 50th percentile models were then scaled to match the

maximum isometric strength of the model for each of the target strengths. This was done using the same approach as was used to scale the models' neck muscle strengths to average strengths [16]. This provided the scale factors needed to scale the 50th percentile models to each of the target strengths. An 8th-order polynomial was then fit to the relationship between muscle scale factor and target strength. This produced a set of equations to compute the scale factor needed to continuously scale the flexor and extensor muscles of the male and female models to a target strength percentile.

Simulations of walking, running, and a static prone posture were then implemented. These activities were selected to capture a range of common warfighter activities. The kinematics and ground reaction forces for walking were obtained from an open-access repository [19]. The kinematics and ground reaction forces for running were collected from participants running at a self-selected speed on a level treadmill [20]. For both activities, data were selected from participants that were closest to the height and weight of the 50th percentile models. The 50th percentile models were then were scaled to the representative participant anthropometry [13]. Synthetic data were generated to simulate static prone. The kinematics for this posture were defined by positioning the 50th percentile models into a generic prone posture. Joint definitions at the elbow, wrist, hip, knee, and ankle joints were then locked, keeping only the necessary joints in the head-neck region active. The ground reaction force was calculated as the weight of the model and applied to the whole body's centre of mass (CoM). For all three activities, the joint angles and ground reaction forces were used as input to a residual reduction algorithm and CMC simulations in OpenSim [13, 17]. The CMC simulations generated estimates of muscle activations and forces for the neck muscles and joint reaction forces and torques for the cervical spine. Walking and running simulations were conducted over a complete gait cycle. The prone posture was simulated for one second to be similar in duration to the walking and running simulations.

2.2 Muscle Fatigue Model

The ability to model muscle fatigue was implemented to simulate the effect of long-duration missions on MSK burden. The selected muscle fatigue model is based on compartment theory and divides the state of muscle fibres into three categories: "active" and able to exert force, "fatigued" and not exerting force, and "resting," but able to be recruited [21–24]. This model was implemented by defining a new muscle type in an OpenSim plugin that computes the proportion of muscle fibres in each state using the muscle fatigue model and uses the Millard muscle model to simulate muscle mechanics [25]. A "fatigued" and "resting" state were added to the model, in addition to the default "active" state. The changes in muscle state were translated to a change in muscle activation with the following equation:

$$\frac{da}{dt} = \frac{dM_A}{dt} * a_t + M_A * \frac{da_t}{dt} \quad (1)$$

where $\frac{da}{dt}$ is the activation rate of the muscle, $\frac{dM_A}{dt}$ is the rate of change in active muscle fibres, a_t is the target activation from the first-order activation dynamics in OpenSim, M_A is the proportion of muscle fibres in an "active" state, and $\frac{da_t}{dt}$ is the target activation rate. Activation is modelled in OpenSim as a first-order differential equation that "relates the rate of change of muscle activation to the muscle excitation (i.e., the firing of motor units)" [26]. The target activation is, therefore, related through the first-order differential equation to the excitation target that is computed by CMC. Importantly, this modification to account for muscle fatigue does not change the underlying mechanics of the muscle model meaning each muscle still behaves mechanically the same as a Millard muscle model.

2.2.1 Neck Muscle Fatigue Experiments

The implemented muscle fatigue model was designed to generalize to all types of skeletal muscle. This is done by calibrating the fatigue and recovery parameters to accurately capture the muscle fatigue dynamics for a given body region. The parameters of this fatigue model were previously calibrated for multiple body regions, including the shoulder, knee, and elbow, but not the neck [24]. The parameters for modelling neck muscle fatigue were determined through calibration to data from fatigue experiments.

Twenty young, healthy participants volunteered for the neck muscle fatigue experiments (10 male/10 female, 25.7 ± 3.4 years, 172.2 ± 7.5 cm, 70.6 ± 12.0 kg). Eligible participants had no neck pain in the past 3 months (as rated by scoring 4 or less on the Neck Disability Index [27]), performed at least 150 minutes total of moderate exercise per week, and performed strength training at least two days per week. Interested participants were excluded if they had conditions that may have interfered with their ability to safely perform exercise testing. The protocol was approved by the Johns Hopkins University Institutional Review Board and the US Army Human Research Protection Office (IRB00335161). All

https://doi.org/10.52202/081621-0023

participants provided informed consent.

Six isometric maximum voluntary contractions (MVCs) were performed for both neck extension and neck flexion to establish a baseline maximum torque per motion. Participants performed the isometric neck exercises on a Biodex dynamometer (System 4 Pro, Biodex Medical Systems, Inc., Shirley, NY, USA) while seated in a rigid chair that was weighted to the ground. The centre of the dynamometer was aligned with the palpated C7 spinous process of each participant. A custom rigid padded attachment for testing neck muscle strength was developed using a Biodex ankle attachment and a padded fixture. The custom attachment was fit to the Biodex dynamometer arm so that the attachment arm rested against the occipital protuberance for extension and the brow line for flexion (Figure 1). MVC trials consisted of six 10-second cycles. Participants pushed with as much force as possible for the first 7 seconds of each cycle and rested for the last 3 seconds. Biodex data were acquired at 2000 Hz.

Figure 1. Experimental setup to capture torque production. Participants were positioned in the Biodex System 4 in different orientations for extension (left) and flexion (right).

Participants then performed a fatigue protocol that consisted of repeated MVC cycles in extension. Each MVC cycle consisted of a 7-second maximum contraction followed by 3 seconds of rest. Participants repeatedly performed these MVC cycles until either (a) fifteen minutes had passed or (b) participants decided to end the protocol due to fatigue. The Biodex dynamometer and fixture were set up the same as during the MVC extension trials. Before the start of the fatigue protocol, participants were shown a target line of the maximum torque achieved during their baseline extension MVC trials and were encouraged to practice matching peak torque production. Participants were asked to report their rating of perceived exertion (RPE) using the Borg scale [28] immediately before and at the end of each minute of the protocol. At the conclusion of the extension fatigue protocol, participants rested for ten minutes and then were encouraged to complete a neck flexion fatigue protocol. The Biodex dynamometer and fixture were set up the same as for the MVC flexion trials. The flexion fatigue protocol was performed the same as the extension fatigue protocol, but with participants pressing their forehead against the fixture in flexion. Fourteen of the twenty participants performed both the extension and flexion fatigue protocols.

For each trial, the torque produced by the weight of the Biodex arm was subtracted from the measured torque. The torque data were then filtered with a 10th-order low-pass Butterworth filter with a 10 Hz cut-off frequency [29]. A moving average filter with a window size of 200 samples was then applied. For each 7-second cycle, the peak torque and time of peak were extracted. The maximum torque achieved for each fatigue protocol was then used to calculate the percent MVC for each cycle. Percent MVC data were then regularized to 10 Hz by linear interpolation to enable use within the fatigue model solver and comparison with simulated fatigue model results.

2.2.2 Fatigue Model Calibration

The regularized percent MVC data from the fatigue experiments were then used to determine a set of optimal model parameters to describe neck muscle fatigue. This parameter optimization used a simulated annealing routine (MATLAB, Mathworks, Natick, MA, USA) to optimize the fatigue (F), recovery (R), and recovery accelerator (r) parameters within the muscle fatigue model to best fit the percent MVC data for each participant. The optimal model parameters were determined by minimizing the sum of squared errors between the model predicted and experimentally measured normalized torque time histories (Figure 2). This optimization was performed for both the flexion and extension fatigue data for each participant, which resulted in a set of flexor and extensor muscle fatigue parameters for each participant.

Unpaired t-tests were performed to test for differences in the fatigue parameters across loading conditions (i.e., flexion versus extension) and across biological sex (i.e., female versus male). The threshold for significance was set at $p < 0.025$ to account for multiple comparisons. This statistical analysis was performed to evaluate if different fatigue parameters should be used for the flexor and

https://doi.org/10.52202/081621-0023

extensor muscles and for the 50th percentile male and female models within the software application.

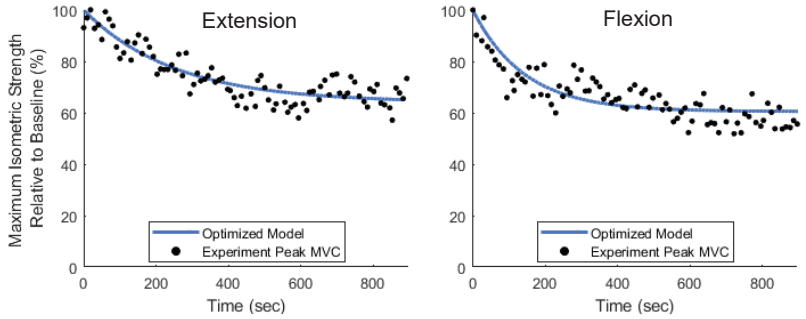

Figure 2. Example model fit for the extension (left) and flexion (right) fatigue data for one participant. The black dots are the peak torque for each MVC as a percent of the maximum torque and are plotted at the time the peak was achieved. The line is the fatigue model with optimized parameters.

A significant difference was found in the extension and flexion fatigue factors ($p < 0.025$, Figure 3). There was no significant difference in the recovery factor and the recovery accelerator across fatigue protocols. Additionally, there was no significant difference in each of the fatigue parameters across biological sex within both the extension and flexion fatigue protocols. This indicated that different fatigue parameters should be used for the extensor and flexor muscles, but that the same fatigue parameters could be used for the 50th percentile female and male models. The final fatigue factor, recovery factor, and recovery accelerator were computed by averaging each of these parameters across participants for the flexors and extensors separately (Table 1).

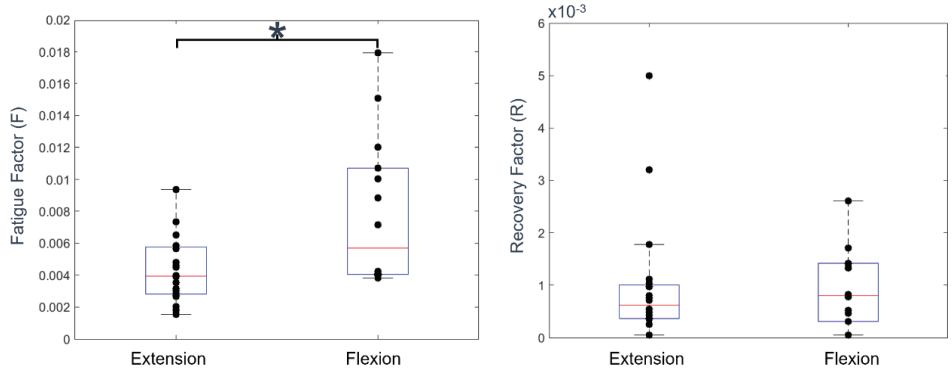

Figure 3. Fatigue factor (left) and recovery factor (right) determined by optimizing the model to the extension and flexion fatigue data. The black dots are the fatigue and recovery factor for each participant. The red lines are the median of the optimized parameters. * indicates a significant difference ($p < 0.025$) in the fatigue factor for the extensors and the flexors.

Table 1. Final fatigue model coefficients calculated for the extensor and flexor muscles

Neck Region	Fatigue Factor (F)	Recovery Factor (R)	Recovery Accelerator (r)
Extensor Muscles	0.003604	0.000347	25.02088
Flexor Muscles	0.006766	0.000867	14.971507

2.2.3 Defining Levels of Fatigue for Software Application

The resultant neck muscle fatigue model was then used to model levels of fatigue within the software application. Four levels of fatigue were selected through input from subject matter experts and potential end-users. The levels of fatigue were modelled by varying the proportion of muscle fibres in the fatigue compartment for each of the neck muscles. Each of the neck muscles are first grouped into a flexor or extensor compartment. The proportion of muscle fibres in the fatigue compartment for each of the muscles are then varied to simulate each of the different levels of fatigue. The remainder of the muscle fibres start in the active compartment at the beginning of a simulation (i.e., 100 minus the proportion of muscle fibres in the fatigue compartment). None of the muscle fibres start in the resting state.

https://doi.org/10.52202/081621-0023

The mapping of proportion of muscle fibres in the fatigue compartment to level of fatigue was developed to align with the neck muscle fatigue experiments. Severe fatigue was set to a 50% reduction from the models' baseline strength based on participants' average maximal reduction in torque generating capacity. This was determined to be a reasonable upper limit of neck muscle fatigue as the fatigue experiments were a very severe loading case for the neck muscles and participants typically reached an "extremely hard" level of exertion (i.e., 18+ on the 20-point Borg RPE scale [28]). Mild and moderate fatigue were then set as equal increments from no fatigue to severe fatigue, with mild and moderate set to reductions of 83% and 67% of baseline strength, respectively.

Mapping from the target reduction in strength to proportion of muscle fibres in the fatigue compartment was then determined through a sensitivity analysis. In this sensitivity analysis, the proportion of muscle fibres in the fatigue compartment was varied from 0% to 75% for the extensors and 0% to 70% for the flexors in 5% increments (Figure 4). The remaining muscle fibres were in the active compartment and none of the muscle fibres were in the resting compartment. The maximum torque generating capacity of the model was then assessed for each of these fatigue levels. A linear regression model was then developed with proportion of muscle fibres in the fatigue compartment as the independent variable and the change in model strength relative to baseline as the dependent variable. This regression model was then used to compute the proportion of muscle fibres in the fatigue compartment needed to induce the target change in model strength for each of the levels of fatigue. This produced the final model states used for each level of fatigue in the software application.

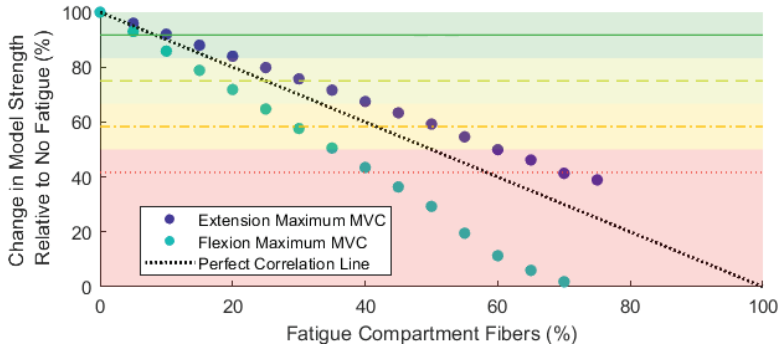

Figure 4. Plot showing the change in maximum isometric strength of the neck, relative to no fatigue, due to changing the proportion of muscle fibres in the fatigue compartment for both the extensors (blue dots) and flexors (turquoise dots). A perfect correlation (black dotted line) and the target changes in strength for each level of fatigue are shown. These results were used to map from target level of fatigue to proportion of muscle fibres in the fatigue compartment.

2.3 Integration into HTAT Software Application

The developed models and analyses were integrated into a software application to evaluate the effect of HBE mass properties, activity, biological sex, and neck muscle strength and fatigue on MSK burden. This software is called the Headborne Equipment Tradespace Assessment Tool (HTAT) and is comprised of simulation (Figure 5), analysis (Figure 6), and help pages. The Simulation Page contains three panels: Setup Properties, Simulation Queue, and Simulation Details. The Setup Properties panel is used to set up and run a model by selecting a biological sex, activity, HBE configuration, neck muscle strength, and level of muscle fatigue. The Simulation Queue is used to visualize the status of simulations that are completed, running, or queued to run. For simulations in the queue, additional information on when the simulation started running, ended (if applicable), and the setup properties are shown to track simulations. Immediately above the Simulation Queue is a progress indicator with a spinning circle to show that the indicated simulation is actively running. The Simulation Details panel contains information on the simulation that is currently running and the simulation that has most recently completed running. This panel also contains a video clip of the activity selected when a simulation starts running.

The Analysis Page allows users to visualize results from successful simulations. Users first load simulations into the Active Simulations Table to use during an analysis session. Users then move through the Add Plot workflow to generate line, bar, or scatter plots based on any subset of the active simulations. Plots may then be modified to adjust the colours, labels, or scaling. Plots can be saved individually or as a group to a user selected folder. Data in the plots may also be exported to a Microsoft Excel file for inspection or development of different plots. Together, the simulation and analysis page allow users to evaluate the effect of HBE on warfighter burden.

https://doi.org/10.52202/081621-0023

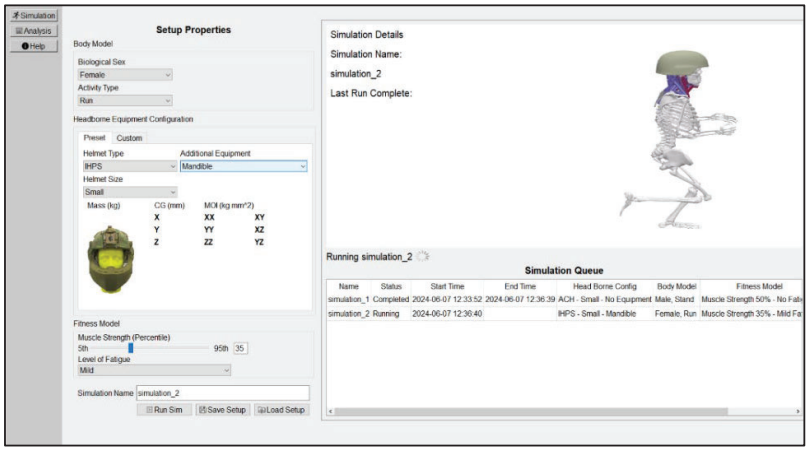

Figure 5. The simulation page within HTAT is used to setup, run, and monitor progress of simulations

Figure 6. The analysis page within HTAT is used to visualize the results of successful simulation runs. Visualizations and the associated data can also be exported within this page.

3. INVESTIGATING THE EFFECT OF HBE DESIGN ON WARFIGHTER BURDEN

The effect of HBE mass properties on warfighter burden was then investigated using HTAT. Previous studies have found that HBE mass properties and activity being performed affect neck pain, cervical spine mechanics, and muscle fatigue [9]. However, this research focused on a well-rested 50th percentile male and analysed relatively simple movements. This limits our understanding of how variations across warfighters during functional activities interact with HBE to further impact MSK burden. Thus, the goal of this investigation was to perform a preliminary analysis of the effect of HBE mass properties and muscle fatigue on MSK burden, while considering warfighter variations as a potential use-case of HTAT.

3.2 Methods

Using HTAT, we analysed the effect of variations in HBE mass, CoM, and muscle fatigue for male and female walking. A HBE configuration fielded within the United States Army was selected as the base configuration for varying HBE mass properties. The following variations were simulated relative to this configuration: (1) varying the HBE mass from 1 kg to 4 kg with a constant CoM and (2) varying the CoM from 2 cm posterior to 10 cm anterior relative to the head CoM with a constant HBE mass of 2 kg. These ranges were selected to encompass the mass and anterior-posterior CoM location of fielded equipment [30]. Walking simulations were performed with each of the variations in HBE mass properties for the female and male models. For variations in fatigue, walking simulations were performed at each level of fatigue with the female and male 50th percentile models and the base HBE configuration.

The joint reaction forces were computed within HTAT as the result of all forces acting at each

https://doi.org/10.52202/081621-0023

joint, including muscle forces [31]. The resultant joint reaction force at T1-C7 was then integrated across time for each simulation to compute the joint impulse. The change in joint impulse relative to the lowest mass configuration was computed for simulations with varying HBE mass. The change in impulse relative to a CoM aligned with the head CoM was computed for simulations with varying CoM. The change in impulse relative to no fatigue was computed for simulations with varying levels of fatigue.

3.3 Results

Increasing the HBE mass and shifting the CoM location anterior led to an increase in joint impulse at T1-C7 for both the male and female models (Figure 7). Joint impulse increased by 105 Ns and 57.2 Ns for the male and female models, respectively, across the range of simulated HBE mass. Joint impulse increased by 18.6 Ns and 61.1 Ns for the male and female models, respectively, across the range of CoM locations. However, the change in joint impulse was relatively small for the male model (i.e., less than 5 Ns) when the CoM location was between 2 cm posterior to 4 cm anterior. Shifting the CoM posterior led to a decrease in joint impulse for the female model.

Increasing fatigue increased the joint impulse for both the female and male model (Figure 8). Joint impulse increased by 61.4 Ns for the male model and 43.0 Ns for the female model from no fatigue to severe fatigue.

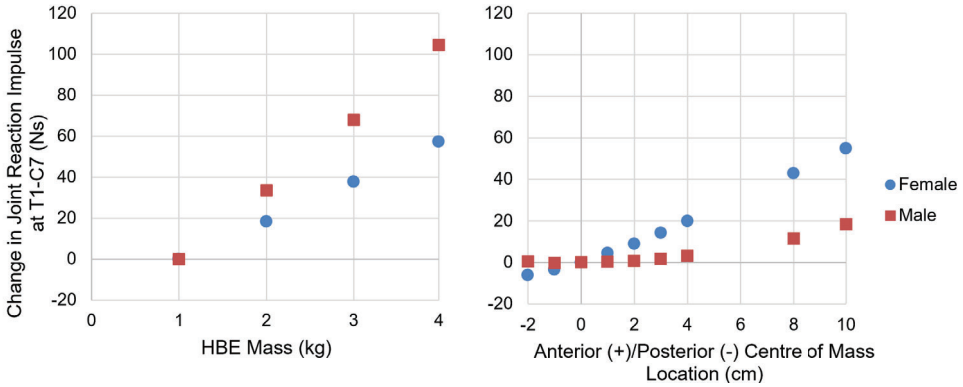

Figure 7. Effect of HBE mass (left) and anterior-posterior CoM location on the change in joint impulse at T1-C7 during simulated walking. This change was computed relative to the lowest HBE mass (i.e., 1 kg) or a CoM aligned with the head CoM. Blue dots are simulations with the 50th percentile female model and red squares are simulations with the 50th percentile male model.

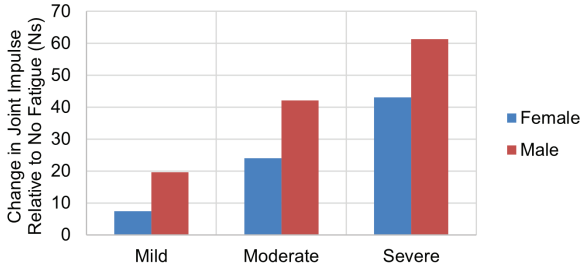

Figure 8. Change in joint impulse relative to no muscle fatigue for mild, moderate, and severe fatigue

4. DISCUSSION AND CONCLUSIONS

The goal of this project was to develop a software application to evaluate the effect of HBE on warfighter burden across a range of warfighters. This was done by first extending an existing MSK model to simulate differences across equipment and warfighters by incorporating variations in HBE, biological sex, activity, strength, and muscle fatigue. These updated MSK models and analyses were then integrated into the Headborne Equipment Tradespace Assessment Tool (HTAT). This application evaluates the effect of simulated variations in HBE mass properties, 50th percentile height and weight (through variations in biological sex), activity, neck muscle strength, and neck muscle fatigue on MSK burden. This provides a number of use cases, including (1) evaluating differences in MSK burden across existing

https://doi.org/10.52202/081621-0023

HBE configurations or new HBE designs, (2) evaluating differences in MSK burden across a population with varying strength and stature for a given HBE configuration, (3) understanding changes in MSK burden across a mission due to increased muscle fatigue, and (4) assessing how activities performed by warfighters may elevate MSK burden when wearing HBE. Each of these use cases can be used to help inform guidance for HBE mass properties during dismounted operations.

The effect of HBE mass and anterior-posterior CoM location on MSK burden was investigated using HTAT. Increased HBE mass and a more anterior CoM led to increased joint impulse in the cervical spine. This is consistent with previous studies indicating that varying HBE mass and CoM location can alter neck pain, discomfort, and muscular fatigue [1–4]. The results from HTAT expand upon these previous findings to allow the change in joint impulse with varying HBE mass properties to be quantified, which could inform objective guidance on HBE mass properties. Improved understanding of the relationship between these biomechanical metrics and risk of injury or changes in performance would help establish thresholds for HBE design. The change in joint impulse was relatively small for the male model when the CoM was between 2 cm posterior to 4 cm anterior. This may be due to greater strength of the male model resulting in a reduced sensitivity to variations in HBE CoM. Shifting the HBE CoM posterior led to reduced joint impulse for the female model. However, we cannot extrapolate this effect to a CoM beyond the range that was simulated. The range in joint impulse was greater for variations in HBE mass than for CoM. While a single unit change in HBE mass and CoM are not equivalent, this suggests that reducing HBE mass may provide greater benefit to reducing warfighter burden.

Increasing the level of fatigue increased cervical spine joint impulse for both 50^{th} percentile models. This indicates that, as warfighters become more fatigued during a mission, biomechanical changes occur that may increase likelihood of neck injury. Additionally, the range in joint impulse was similar magnitude when varying levels of fatigue and varying HBE mass properties. While there is no way to directly compare changes in muscle fatigue and changes in mass properties, this suggests that level of fatigue and, thus, duration a warfighter is wearing a HBE configuration, could contribute to neck injury risk and is likely important to consider when developing guidance for HBE mass properties.

When interpreting results from HTAT, it is important to consider the following limitations. First, the current models do not account for changes in movement patterns that may occur due to differences in HBE or fatigue. This allows users to understand biomechanical changes that would occur if a warfighter maintained the same movement pattern across different HBE. However, the ability to evaluate changes in movement patterns could be implemented through use of predictive MSK models [32]. Next, the male and female models differ in height, weight, neck muscle strength, and self-selected walking and running speeds. This makes it challenging to assess the specific factor driving differences in outcomes between these models. Implementing the ability to control variations in anthropometrics across a range of movement dynamics would improve understanding of the effect of these parameters on MSK burden. Finally, there is no direct mapping between the metrics evaluated in HTAT and injury risk or changes in performance. Future work will investigate the relationship of biomechanical and other model-based metrics with neck injury risk and changes in performance to improve interpretability.

In conclusion, we developed a software application to evaluate the effect of HBE mass properties on MSK burden across variations in warfighter stature, weight, strength, and fatigue and across a range of activities. This application can be used within armour acquisition, design, and test and evaluation to support assessments of the tradespace of warfighter protection, performance, and injury risk offered by HBE. Using this application, we found that variations in HBE mass properties and level of fatigue led to increases in MSK burden. This indicates that HBE mass properties, variations across warfighters, and mission duration should all be considered when developing guidance for design and use of HBE.

Acknowledgments

The authors would like to thank Program Executive Office Soldier Product Manager Soldier Protective Equipment for sponsoring this effort. The authors would also like to thank Marina Carboni at US Army Combat Capabilities Development Command Soldier Center for measuring the mass properties of the HBE configurations in HTAT. Any opinions, findings and conclusions or recommendations expressed in this material are those of the author(s) and do not necessarily reflect the views of PEO Soldier, DEVCOM Soldier Center, or Naval Sea Systems Command.

References

[1] Tack D. W., Nakaza E. T., McKee K. W., MacEachern C. A., and Marrao C. C., Investigation of the Preferred Mass Properties for Infantry Headwear Systems, Humansystems Incorporated, DRDC Toronto CR-2005-230, (2006).

[2] Knight J. F. and Baber C., Neck muscle activity and perceived pain and discomfort due to variations of head load and posture, *Aviat Space Environ Med*, 75(2), pp. 123–131, (2004).

https://doi.org/10.52202/081621-0023

[3] Madison A., Preliminary Head-Supported Mass (HSM) Performance Guidance for Dismounted Soldier Environments, USAARL Technical Memorandum 2019-11, (2019).
[4] Madison A. M. *et al.*, Preliminary Head-Supported Mass Performance Guidance for Dismounted Soldier Environments, *Military Medicine*, 188(Supplement_6), pp. 520–528, (2023).
[5] Lim J. *et al.*, Additional helmet and pack loading reduce situational awareness during the establishment of marksmanship posture, *Ergonomics*, 60(6), pp. 824–836, (2017).
[6] Gallagher H. L., Caldwell E., and Albery C. B., Neck Muscle Fatigue Resulting from Prolonged Wear of Weighted Helmets, AFRL-RH-WP-TR-2008-0096, (2008).
[7] Butler B. P. and Allen N. M., Long-Duration Exposure Criteria for Head-Supported Mass, ARMY AEROMEDICAL RESEARCH LAB FORT RUCKER AL, (1997).
[8] McEntire B. J. and Shanahan D. F., Mass Requirements for Helicopter Aircrew Helmets, ARMY AEROMEDICAL RESEARCH LAB FORT RUCKER AL, (1997).
[9] Barrett J. M., Healey L. A., Fischer S. L., and Callaghan J. P., Cervical Spine Motion Requirements From Night Vision Goggles May Play a Greater Role in Chronic Neck Pain than Helmet Mass Properties, *Hum Factors*, p. 001872082210906, (2022).
[10] Cazzola D., et al., Cervical Spine Injuries: A Whole-Body Musculoskeletal Model for the Analysis of Spinal Loading, *PLOS ONE*, 12(1), (2017), doi: 10.1371/journal.pone.0169329.
[11] Silvestros P. *et al.*, Musculoskeletal modelling of the human cervical spine for the investigation of injury mechanisms during axial impacts, *PLoS ONE*, 14(5), p. e0216663, (2019).
[12] Silvestros P., *et al.*, Electromyography-Assisted Neuromusculoskeletal Models Can Estimate Physiological Muscle Activations and Joint Moments Across the Neck Before Impacts, *Journal of Biomechanical Engineering*, 144(3), p. 031011, (2022), doi: 10.1115/1.4052555.
[13] Seth A. *et al.*, OpenSim: Simulating musculoskeletal dynamics and neuromuscular control to study human and animal movement, *PLOS Computational Biology*, 14(7), p. e1006223, (2018).
[14] Gordon C. C. *et al.*, 2012 Anthropometric Survey of U.S. Army Personnel: Methods and Summary Statistics, U.S. Army Natick Soldier Research, Development and Engineering Center, Natick, (2014).
[15] Roos P. E., Vasavada A., Zheng L., and Zhou X., Neck musculoskeletal model generation through anthropometric scaling, *PLoS ONE*, 15(1), pp. 1–21, (2020).
[16] Mortensen J. D., Vasavada A. N., and Merryweather A. S., The inclusion of hyoid muscles improve moment generating capacity and dynamic simulations in musculoskeletal models of the head and neck, *PLOS ONE*, 13(6), p. e0199912, (2018), doi: 10.1371/journal.pone.0199912.
[17] Thelen D. G., Anderson F. C., and Delp S. L., Generating dynamic simulations of movement using computed muscle control, *Journal of Biomechanics*, 36(3), pp. 321–328, (2003).
[18] Vasavada A. N., Li S., and Delp S. L., Influence of Muscle Morphometry and Moment Arms on the Moment-Generating Capacity of Human Neck Muscles, *Spine*, 23(4), p. 412, (1998).
[19] Moore J. K., Hnat S. K., and Bogert A. J. van den, An elaborate data set on human gait and the effect of mechanical perturbations, *PeerJ*, 3, p. e918, (2015), doi: 10.7717/peerj.918.
[20] Vignos M. F. *et al.*, Physical Fatigue State Classification through Fusion of Physiological and Biomechanical Metrics, presented at the 2023 International Congress on Soldiers' Physical Performance, London, UK, Sep. 12, 2023.
[21] Liu J. Z., Brown R. W., and Yue G. H., A Dynamical Model of Muscle Activation, Fatigue, and Recovery, *Biophysical Journal*, 82(5), pp. 2344–2359, (2002).
[22] Xia T. and Frey Law L. A., A theoretical approach for modeling peripheral muscle fatigue and recovery, *Journal of Biomechanics*, 41(14), pp. 3046–3052, (2008).
[23] Looft J. M. and Frey-Law L. A., Adapting a fatigue model for shoulder flexion fatigue: Enhancing recovery rate during intermittent rest intervals, *J Biomech*, 106, p. 109762, (2020).
[24] Frey-Law L. A., Looft J. M., and Heitsman J., A three-compartment muscle fatigue model accurately predicts joint-specific maximum endurance times for sustained isometric tasks, *Journal of Biomechanics*, 45(10), pp. 1803–1808, (2012), doi: 10.1016/j.jbiomech.2012.04.018.
[25] Millard M., *et al.*, Flexing Computational Muscle: Modeling and Simulation of Musculotendon Dynamics, *Journal of Biomech Eng*, 135(021005), (2013), doi: 10.1115/1.4023390.
[26] Millard M., Seth A., and Loan P., First-Order Activation Dynamics, 2012. https://simtk-confluence.stanford.edu:8443/display/OpenSim/First-Order+Activation+Dynamics.
[27] Vernon H., The Neck Disability Index: State-of-the-Art, 1991-2008, *Journal of Manipulative and Physiological Therapeutics*, 31(7), pp. 491–502, (2008), doi: 10.1016/j.jmpt.2008.08.006.
[28] Williams N., The Borg Rating of Perceived Exertion (RPE) scale, *Occupational Medicine*, 67(5), pp. 404–405, (2017), doi: 10.1093/occmed/kqx063.
[29] Nordez A., Casari P., and Cornu C., Accuracy of Biodex system 3 pro computerized dynamometer in passive mode, *Medical Engineering & Physics*, 30(7), pp. 880–887, (2008).
[30] Estep P. N. *et al.*, Mass Properties Comparison of Dismounted and Ground-Mounted Head-Supported Mass Configurations to Existing Performance and Acute Injury Risk Guidelines, *Military Medicine*, 184(Supplement_1), pp. 245–250, (2019), doi: 10.1093/milmed/usy342.
[31] Steele K. M., DeMers M. S., Schwartz M. H., and Delp S. L., Compressive tibiofemoral force during crouch gait, *Gait & Posture*, 35(4), pp. 556–560, (2012).
[32] De Groote F. and Falisse A., Perspective on musculoskeletal modelling and predictive simulations of human movement to assess the neuromechanics of gait, *Proceedings of the Royal Society B: Biological Sciences*, 288(1946), p. 20202432, (2021), doi: 10.1098/rspb.2020.2432.